Earthen claddings in lightweight timber framed buildings: An experimental study on the influence of fir boards sheathing and GFRP jacketing

Earthen claddings in lightwood framed buildings: an experimental study on the influence of fir boards sheathing and GFRP jacketing

M. Serpilli, F. Stazi, G. Chiappini, S. Lenci

Abstract
The aim of this research was to investigate the mechanical performance of an earthen massive cladding, recently used for external/internal layers in Platform Frame technology, through an extensive experimental campaign. The masonry is built with extruded unbaked earth blocks and characterized by dovetail horizontally staggered bed joints. The wall is secured to the structural timber studs through 45 degree-angled fir boards sheathing panels, fixed with steel connectors, and finished with an external plaster with an embedded Glass Fibre Reinforced Polymer (GFRP) mesh, wrapping the whole masonry. The influence of the fir board panels and GFRP jacketing on the mechanical behavior of the earth blocks masonry is investigated and compared with the results obtained for the unreinforced configuration (bare wallettes) in [1]. The experimental program consisted of compression, diagonal compression and combined shear-compression tests on 18 wallettes. Digital Image Correlation technique was also adopted to investigate the full field strain maps. The results showed that under compression all the samples (with and without reinforcements) behave as a series of independent slender columns, without significant differences among reinforcement type. Both diagonal compression and shear with compression tests revealed the optimal behavior of GFRP plaster reinforcement that increase the strength values and thanks to an effective confinement effect, limits the out-of-plane bending and determines a monolithic response of the wall.

1.Introduction

The Platform-Frame technology is a light-framed wooden construction system. It is based on the assembly of walls and floors with a timber frame, composed of evenly spaced structural vertical timber studs and sheathing wall panels (commonly plywood or OSB panels). Insulation typically occurs within the wood studs space [2]. Recently, this kind of construction evolved to satisfy new energy saving requirements by strongly increasing the insulation thickness (using wider studs to provide space for more insulation) and introducing other insulation and massive layers on both sides of the timber paneled structures.

Various experimental researches have been carried out to investigate the behavior of light timber-based systems under in-plane horizontal loads, also by varying the studs and sheathings types and geometric setting [3]. Indeed, the sheathing material revealed to have a major influence on the behavior of the wall. Some authors found that placing an OSB panel in the internal and external sides of the wooden frame confers high stiffness and resistance to deformation [4]. Instead, fiber gypsum sheathing panels were observed to perform poorly during the cyclic tests ([5] and [6]).

In the present study, the bracing sheathing wall panels, made of 45 degree-angled fir boards, are connected to the structural timber studs by means of ring-shank nails. Massive claddings, made of unbaked and extruded earth blocks, are secured to both external and internal fir board panels through metal anchors (Fig. 1). As shown in Fig. 1, the external earthen cladding presents a finishing plaster (based on lime, clay, silt and sand). To enhance mechanically the structural performance of the wall, in some applications a GFRP mesh is embedded within the plaster and fixed to the upper and lower timber beams by means of metal connections. Other details on assembly method for the wallets construction can be found in [1].

While the load-bearing platform framed structures were widely investigated, the mechanical behavior of the massive external and internal layers fixed to the studs or to the sheathing panels was rarely surveyed. This aspect is novel since only in recent years the lightweight wooden techniques have been combined with massive claddings in response to the newly born problems of indoor overheating of super-insulated wooden envelopes [7]. Numerous studies were carried out on bare earth block wall specimens or on small samples of timber frames with brick infills in order to characterize the mechanical behavior and tune numerical models, see e.g. [8], [9]. Also, a previous paper of our research group [1] focused on the mechanical characterization of an earth block masonry to evaluate possible application for load bearing functions. The experimental activity envisaged experimental tests on the bare masonry without considering any effect due to the connection with the underlying sheathing panels and the presence of an eventual GFRP jacketing.

The researches, focused on the one-side application of adjunctive reinforcement layers to the bare walls, such as FRP [10]–[12], timber panels [13] or Cross-Laminated Timber (CLT) panels [14], mainly regarded brick and stone masonries for retrofit purposes, and strength and lateral load capacity enhancement. Studies on unbaked earth blocks walls are still lacking.

The present paper aims at contributing to fill this open issue by evaluating the influence of one-sided fir board panels and GFRP mesh on the masonry mechanical performance. To that aim, an experimental survey was carried out involving compression, diagonal compression and shear tests on wallettes, with the application of either a fir board sheathing or a GFRP jacketing. This will reveal the separate contribution of each constructive element, giving, in turn, indications of their influence on the overall timber structure behavior. Moreover, since the fir board sheathing increases the manufacturing complexity and costs in Platform framings, a sub goal is verifying the possibility to replace it using the sole external GFRP jacketing, wrapping the whole masonry.

Digital image correlation (DIC) is adopted for the strain measurements. Indeed, the standard test methods are based on the use of contact sensors, commonly LVDT and strain gauges and the failure mapping can be obtained only through visible survey. DIC allows correlating the crack pattern to the strength values regarding the collapse mechanism and obtaining the full-field strain maps ([1] and [15]).

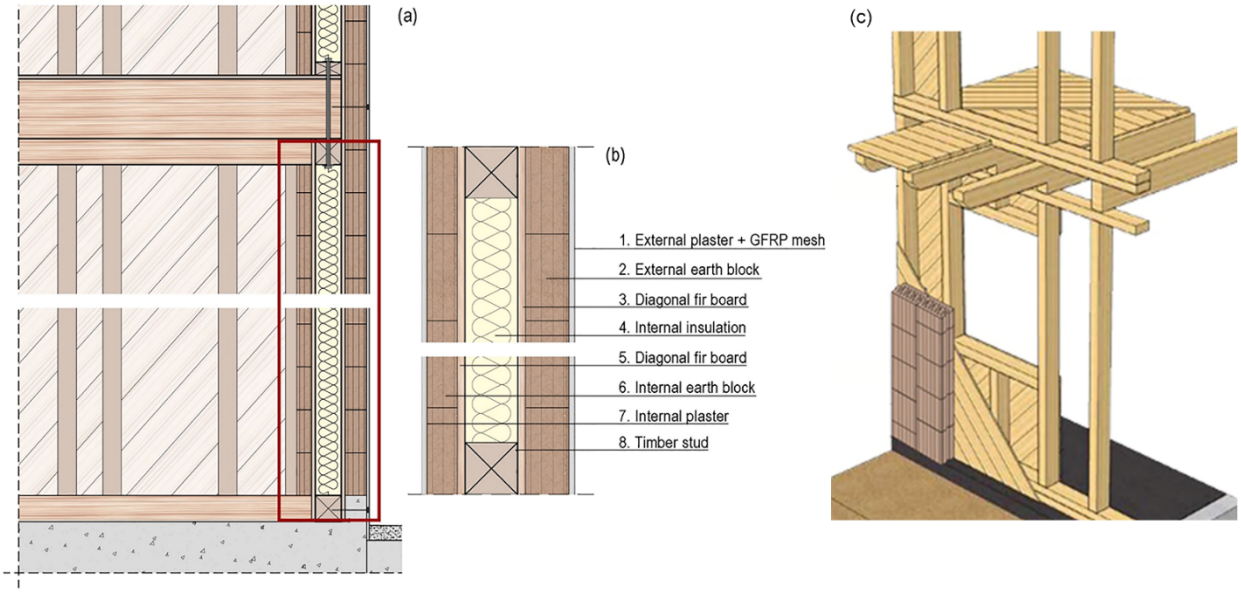

Figure1. (a) Platform-frame assembly technology, (b) envelope layers succession and (c) 3D view

2. Experimental program

2.1 Stages

The research focused on the mechanical properties of three different types of wallettes: (i) bare earth block panels, (ii) earth block panels reinforced through diagonal fir boards (FB) using mechanical fasteners (iii) earth blocks panels with an external plastered GFRP net anchored with threaded rods to the main studs. Table 1 presents the outline of the lab tests.

Table 1. Overview of the lab tests on wallettes.

Test method	Standards/Reference	Specimen description	Specimen
Compressive strength	UNI EN 1052-1:2001	earth block wallette	3
		earth block wallette + FB	3
		earth block wallette + GFRP plaster	3
Diagonal tensile strength	ASTM E519-07	earth block wallette	3
		earth block wallette + FB	3
		Nude earth block wallette + GFRP plaster	3
Tensile strength with compression load	[1] and [16]	earth block wallette	3
		earth block wallette + FB	3
		earth block wallette + GFRP plaster	3

2.2 *Materials and wallettes assembly*

The masonry wall of the present study is made of unbaked extruded hollow earth blocks supplied by Ton-Gruppe, an Italian construction company. The material has a density of 1450 kg/m^3 and it is a mixture of clay

(70%) as the main matrix and spoils of rice husk fibers (30%) as natural stabilizers. The samples consisted of 35 wallettes of dimension 1.1 m x 1 m x 0.1 m.

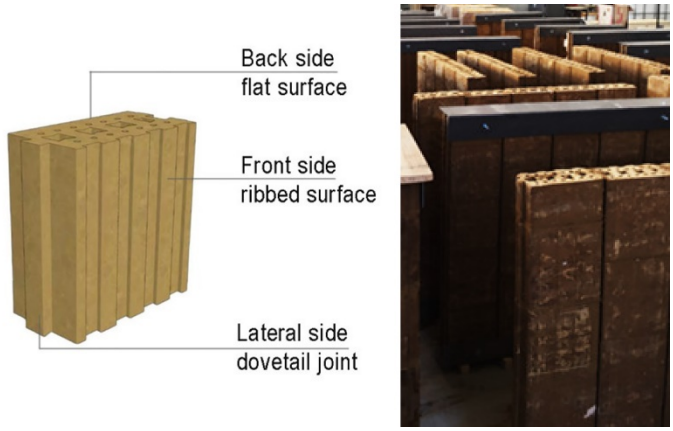

Fig.2. Earth block unit and wallette samples curing in laboratory environment.

The masonry unit (Fig.2) is firstly extruded through a die machine and then is left naturally air-dried. Each block has nominal dimensions of 215 x 230 x 115 mm^3 and presents a flat vertical surface on one side and a ribbed one on the other to provide better adhesion of the external plaster. The lateral surfaces are characterized by dovetail joints which serve as a guide for the alignment of the masonry units during the wall assembly and ensure their mechanical connection, thus enhancing the overall global shear behavior.

The blocks are aligned along vertical columns and are linked together through the aforementioned dovetail joints. The wallets realization comprised the following steps: (i) clay was mixed with water in a ratio of 2:1; (ii) the lateral and the bottom surfaces of each block were uniformly wetted in this paste; (iii) each block was then secured to the others by vertically sliding it along their dovetail joints, thus creating 5 connected vertical piers.

In order to survey the contribution on the overall structural behavior of the bare earth blocks panel and of the earth block panel strengthened with fir board or external GFRF jacketing, three specimen types were built:

- Specimens Type A: bare earth blocks wallettes (Fig. 3a);
- Specimens Type B: earth blocks wallettes with the bracing fir boards and timber studs behind it (Fig. 3b);
- Specimens Type C: earth blocks wallettes with a bio-cement plaster reinforced with GFRP mesh (Fig. 3c).

The characterization of the mechanical behavior of the bare wallettes (type A) have already been investigated in a previous paper [1]. The obtained results have been used as a reference case for comparisons. Components such as fir boards and GFRP reinforced plaster are instead representative of the “as-built” configuration and were studied separately to identify the contribution of each one to the global mechanical behavior of the wallettes.

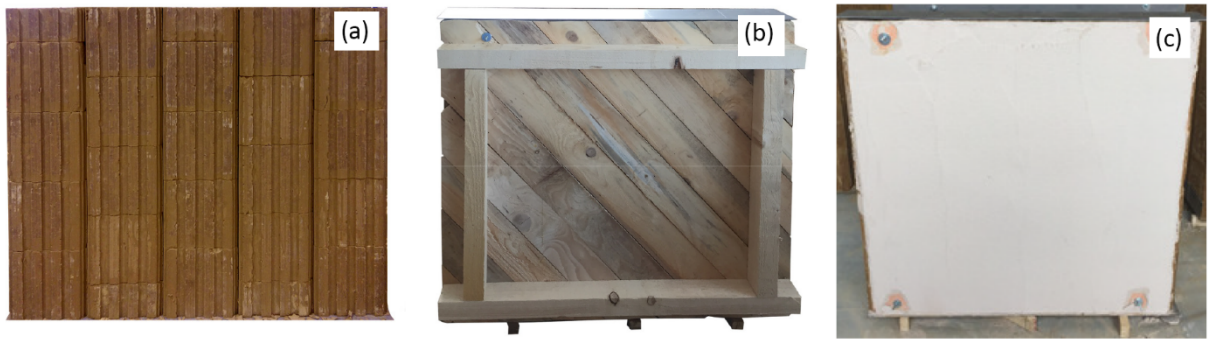

Fig. 3. Three specimen types: (a) bare earth blocks; (b) Fir Boards strengthening and (c) GFRP plaster strengthening

In the selected technology (Fib. 1), the earth wall is supported by a lower beam and fixed to the fir board through distributed feedthrough steel connectors (1ϕ6/m^2). In the external side, the GFRP mesh is secured to the earthen wall through the same distributed metal anchors (1ϕ6/m^2) and fixed to the timber beams at the lower and upper floor levels.

In order to reproduce this application, two L-shaped 3 mm thick steel profiles were mounted at top and bottom side of each sample and used to fix the fir boards (for type B) and the GFRP mesh (for type C) to the assembly with steel connectors (see Fig.4).

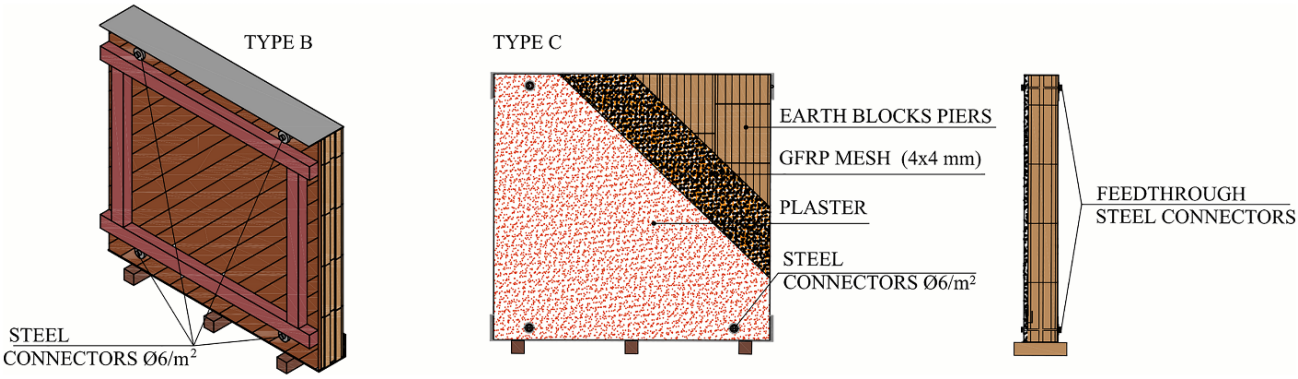

Fig. 4. Details for fir boards and GFRP connections to earth blocks: type B and type C specimens.

The features and strength parameters of the adopted components are reported in Table 2.

All materials and assemblies were stored in the laboratory until testing and the curing process lasted 30 days in a controlled laboratory environment.

Table.2. Components features.

GFRP mesh	
Specific weight	165 g/m^2
Mesh grid sizes	4.0 x 4.0 mm
Failure tensile load in standard conditions	1900/1800 N/50mm (EN 13934-1)
Mortar	
Relative density of powder	1850 kg/m^3

Compressive strength (28 days)	2.5 N/mm^2
Timber (boards and studs)	
Boards thickness	20 mm
Boards width	120 mm
Timber studs sizes	60 x 60 x 1035 mm
Steel Connectors ϕ6/m^2 length	200 mm
Nails to fix timber studs to fir boards, ϕ3/10 cm, length	50 mm

2.3 Tests methods

2.3.1 DIC Set-up

The displacement and deformation of the surface of the wallettes were measured using the 3D-DIC technique. The region of interest (ROI) of the wallettes has been spray-painted with black and white texture. Preliminary tests were carried out to define the most suitable dimensions and intensity of the pattern, following [17]. The experimental set-up is presented in Fig. 5. For further details on the cameras (Fig.5) and calibration data the reader could refer to [1]. During the tests, the manometer was coupled with an additional high-resolution camera that acquired the frames needed to register the pressure trend against time. Then, the values of compression and tensile strengths have been evaluated following the relative test standards.

The pictures of the wallettes acquired during the tests have been post-processed by a 3D-DIC software. The correlation method between the two cameras and the deformed images as well as the error minimization follows the approach described in [1] and [18].

The strains (ε_x, ε_y, and γ_{xy}) have been computed by means of the Cauchy-Green theory, starting from the 3D node displacements [19].

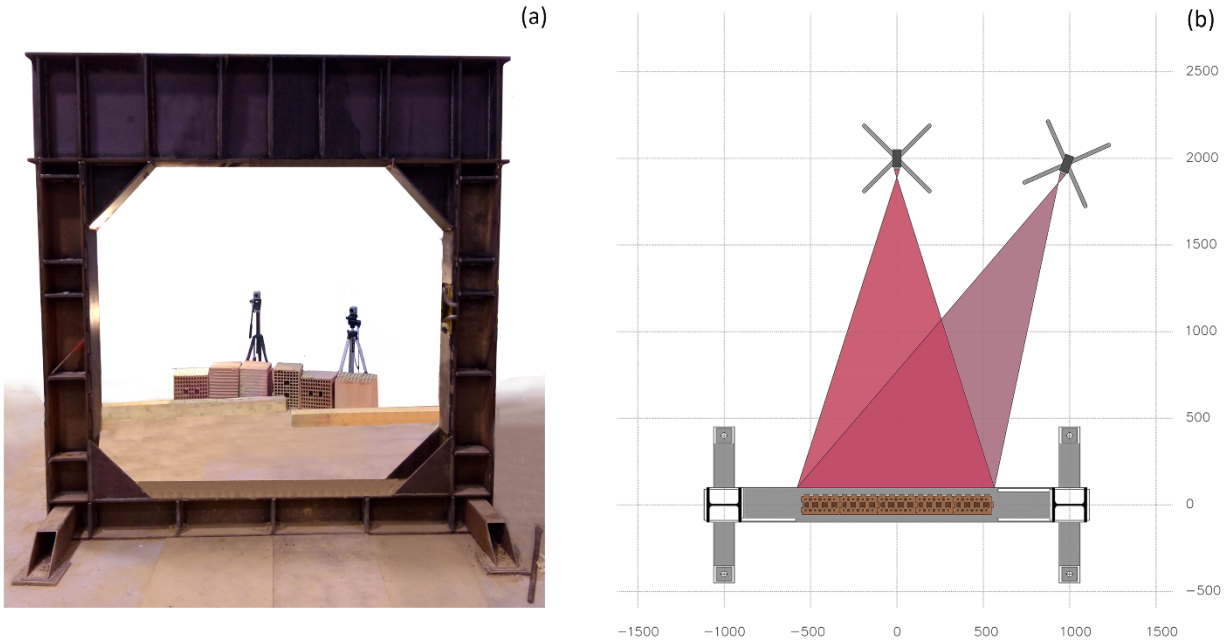

Fig. 5. DIC Set up

2.3.2 Tests on wallettes

The compressive strength of the wallettes (Fig. 6) was determined according to UNI EN 1052-1, on 9 samples (3 samples for each specimen A, B and C). The specimens were tested under axial compression by means of two 500 kN hydraulic jacks, uniformly distributed thanks to a 25 mm-thick steel plate. The steel plate was designed to engage the fir boards (Type B) and external jacket (Type C) in the load application. The nominal strains ε were obtained by averaging the values measured through DIC on the region of interest (ROI).

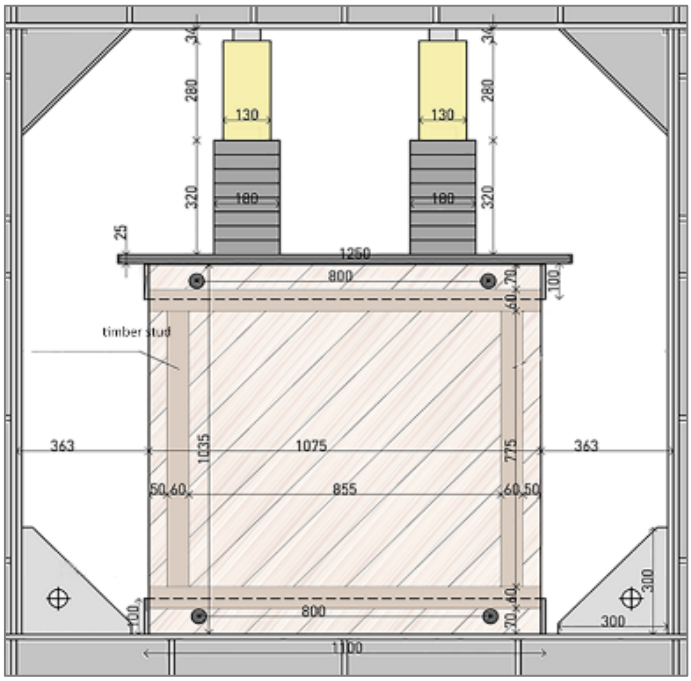

Fig. 6. Tests set-up of the earth masonries under a compression load

The shear strength of the wallettes (Fig. 7) was obtained through diagonal compression tests according to the ASTM E519 – 07 standards on 9 samples (3 samples for each specimen A, B and C). The specimens were subject to diagonal compression by means of a single hydraulic jack (500 kN), acting on a horizontal steel plate placed at the top loading corner. The shear strain γ was obtained through DIC, as the mean value of the γ recorded on the ROI.

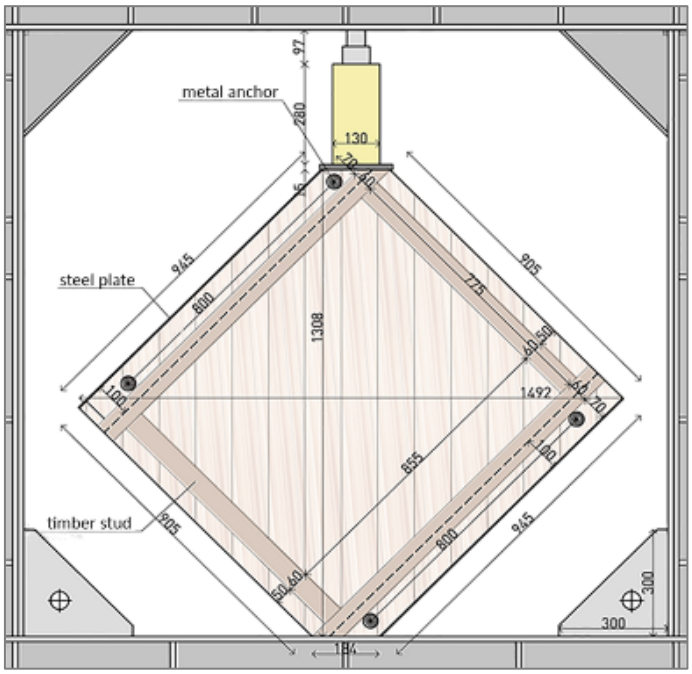

Fig. 7. Tests set-up of the earth masonries under a diagonal compression load

The shear strength of the wallettes under a constant compression load (Fig. 8) was obtained following the experimental procedure adopted by [1], with a compression load of 0.2 N/mm^2. This value was obtained from a preliminary load analysis on a one-story building [20]. A 100 mm x 2.5 mm steel block was welded on the contrast frame, whose function was to block the possible slide of the sample during the test. An "L" shaped steel profile was placed on the upper part of the specimen to transmit the monotonic horizontal force, engaging both fir boards (Type B) and external jacket (Type C) in the vertical and shear load application. A further 25 mm-thick steel plate was then placed above the "L" plate, having care to insert four metal cylinders between them, to allow the sliding between the two plates, to maintain the compression load vertical and to transmit the horizontal force as much as possible by friction. The horizontal force was given by a hydraulic jack, which push on the wall through the "L" plate on the right. It was set up a load cell measuring the amount of force generated by it, connected directly to the horizontal jack. The vertical compression load was directly transmitted by two hydraulic jacks. 9 samples were tested, namely 3 samples for each specimen A, B and C.

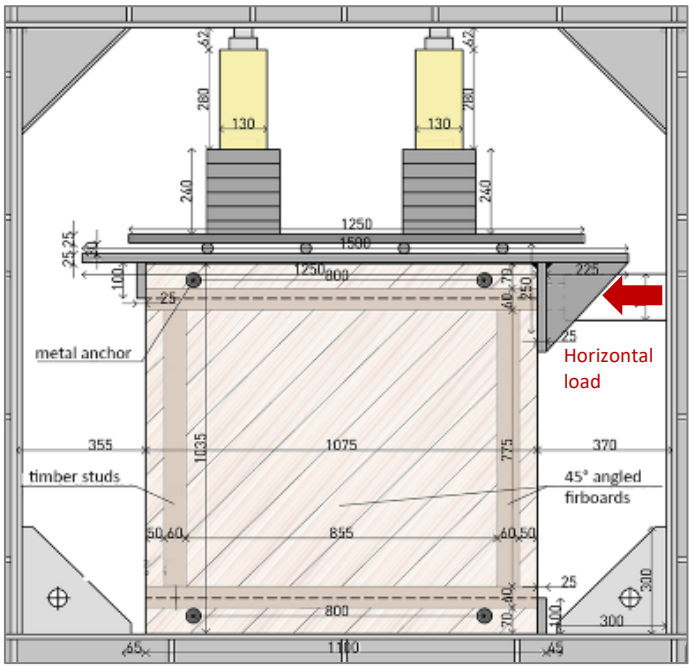

Fig.8. Tests set-up of the earth masonries under a shear with compression load.

The particular board configuration, having their longitudinal fibres along the load application direction, has been adopted in order to maximize the potential contribution under compression and shear of fir boards to stiffness and strength.

The specimens denomination is shown in Table 2.

Table 2. Specimen denomination

Specimen denomination for each test	Bare samples	Fir Board reinforcement	GFRP reinforcement
COMPRESSION TEST	C1, C2, C3	FB-C1, FB-C2, FB-C3	GFRP-C1, GFRP-C2, GFRP-C3
DIAGONAL COMPRESSION TEST	S1, S2, S3	FB-S1, FB-S2, FB-S3	GFRP-S1, GFRP-S2, GFRP-S3
SHEAR TEST WITH COMPRESSION	SP1, SP2, SP3	FB-SP1, FB-SP2, FB-SP3	GFRP-SP1, GFRP-SP2, GFRP-SP3

3. Results

3.1. Compression test results on the wallettes

The stress – strain diagrams (dotted curves) for the 9 wallettes are shown in Fig. 9, where the strain values were obtained through DIC and post-processed in MATLAB. The specimens exhibited an approximately linear behavior up to the maximum load with a brittle failure. Moreover, the mean backbone curves (continuous lines) are plotted in the graph. The compressive strength f_c, Young's modulus determined at 1/3 of maximum stress, E_i and Poisson's ratio ν of the wallettes are summarized in Table 3 and Fig.10. The maximum mean compressive strength value was recorded by the earth blocks + GFRP wallette (2.08 N/mm^2). However, the compressive strength values are of the same order of magnitude among the three specimen types, since this type of action does not significantly activate the strength mechanisms of the reinforcements. The Young's Modulus of the Type B and Type C samples increased with respect to the bare wallettes (Type A) since the

two adjunctive layers, namely the fir boards sheathing and the GFRP jacketing, act as reinforcements contributing to enhance the overall stiffness.

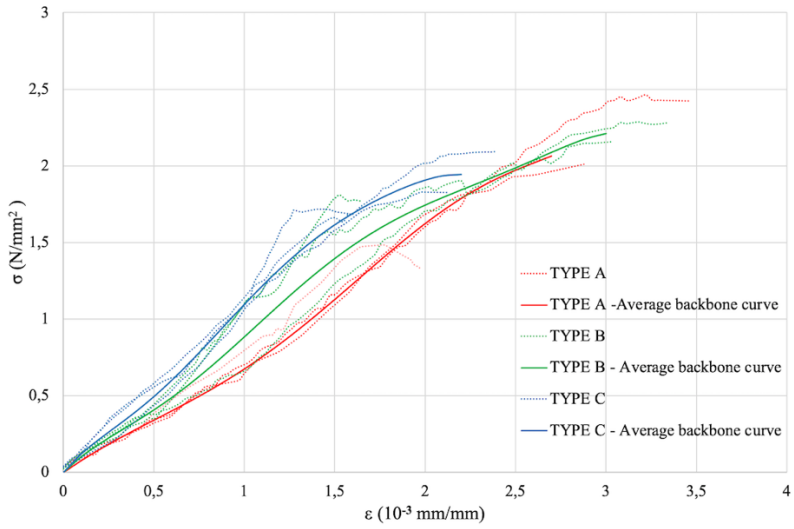

Figure 8. Stress-strain curves of the three types of specimens under compression load.

Table 3. Compressive strength, Young's modulus and Poisson's ratio of the specimens.

Specimen	*fc* (N/mm^2)	E_i (N/mm^2)	ν
C1	2.02	591	0.22
C2	2.46	703	0.23
C3	1.48	740	0.28
Mean values	***1.99***	***678***	***0.24***
COV	***25%***	***11%***	***13%***
FB_C1	1.83	874	0.53
FB_C2	1.72	1024	0.45
FB_C3	2.1	1059	0.49
Mean values	***1.88***	***985***	***0.49***
COV	***10%***	***10%***	***9%***
GFRP_C1	2.29	674	0.30
GFRP_C2	2.16	945	0.28
GFRP_C3	1.81	839	0.39
Mean values	***2.08***	***819***	***0.32***
COV	***12%***	***17%***	***18%***

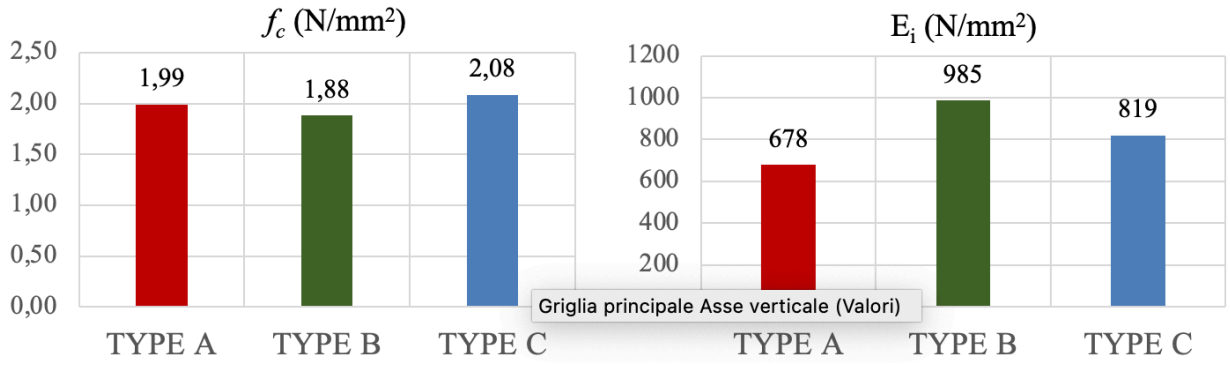

Figure 10. Comparison of (a) the average compressive strengths and (b) Young's Modulus for the three earth masonry specimens under compression load.

The DIC analysis stressed that both the reinforced wallettes were subject to out-of-plane bending: the reinforcement applied on just one side determined a shift of the pressure center. This could explain the slight strength reduction of the wallettes with fir boards (Fig. 11a,b). The technique with external GFRP reinforced plaster could be considered similar to textile reinforced mortars that were found very promising by out of plane tests on brick masonry wallettes ([21] and [22]).

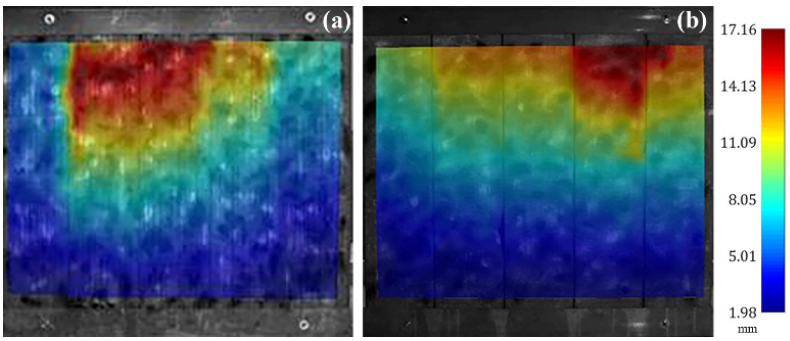

Figure.11. Out-of-plane displacements highlighted through DIC: (a) fir board reinforced specimen and (b) GFRP reinforced specimen

The DIC allowed recovering at each point of the wall the complete displacements and strain fields. For the compression test the vertical displacement s_y map allows to fully understand the mechanical behavior of the wallettes with and without the reinforcements.

From the observation of s_y in the last frame recorded before failure (Fig. 12), it could be noted that all the walls behave as a series of independent slender adjacent columns. Indeed, the alignment of the vertical joints avoids the uniform downward distribution of the load leading to a "column effect" which determined high relative sliding between the vertical members. However, the GFRP reinforced specimens (Fig.12.c) show a better overall response, with a more effective collaboration among contiguous members, as commonly occurs in traditional masonries.

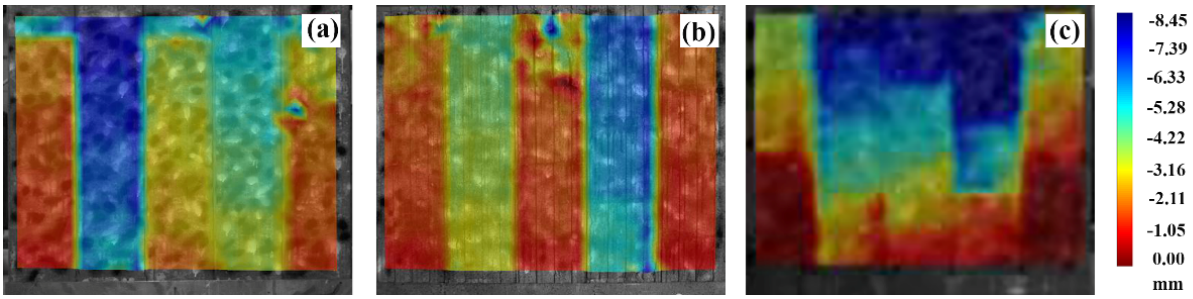

Fig. 12 Vertical displacement ε map under compression obtained through DIC: (a) bare earth block wallette, (b) fir board reinforced specimen and (c) GFRP reinforced specimen

4. Diagonal compression test results on the wallettes

The shear stress–strain curves (dotted lines) for the 9 wallettes are presented in Fig. 13. Moreover, the mean backbone curves (continuous curves) are highlighted in the figure. The curves show a bilinear behavior with great ductility for fir boards reinforcement and high strength increase in GFRP plastered specimens. The tensile strength f_t, secant shear modulus G and secant shear strain γ of the wallettes (both at 1/3 of maximum shear stress), and the ultimate shear strain are reported in Table 4. The bare wallettes specimens showed the lowest tensile strength, with respect to the reinforced ones (Fig. 14a). The strength value f_{im} for the Type B wallettes was 0.051 N/mm^2 while for the Type C Wallette it reached 0.127 N/mm^2. Moreover, the diagonal compression tests highlighted a significant increase of the secant shear modulus for the two reinforced assemblies due to a confinement effect (Fig.14b).

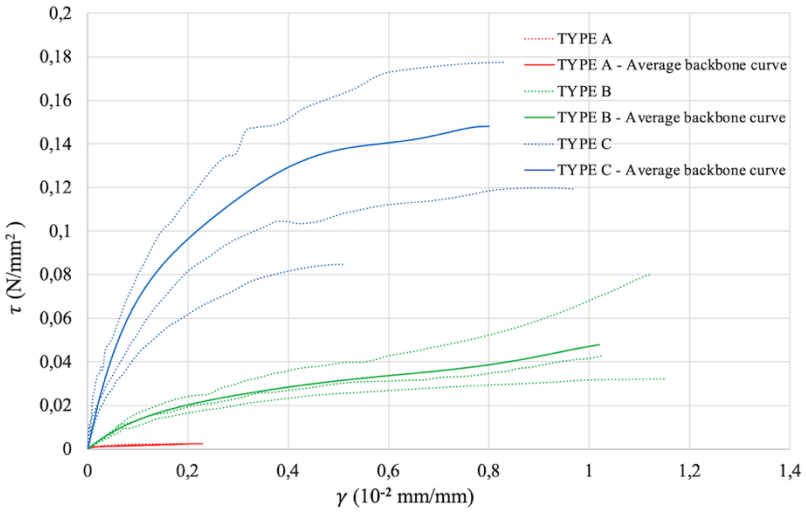

Figure 13. Stress-strain curves of the three types of specimens under diagonal compression load.

Table 4. Tensile strength, secant shear modulus, secant shear strain and ultimate shear strain of the specimens.

Specimen	f_t (N/mm^2)	$G_{1/3}$ (N/mm^2)	$\gamma_{1/3}$	γ
S1	0.00246	7.76	10.57E-05	1.86E-03
S2	0.00236	8.09	9.71E-05	1.91E-03
S3	0.00254	10.2	8.27E-05	2.28E-03

Mean value	***0.00245***	***8.68***	***9.52E-05***	***2.02E-05***
COV	***4%***	***15%***	***12%***	***11%***
FB_S1	0.03216	10.61	1.01E-03	0,011
FB_S2	0.08018	10.50	2.55E-03	0,011
FB_S3	0.04263	12.89	1.10E-03	0,010
Mean value	***0.05166***	***11.33***	***1.55E-03***	***0,011***
COV	***49%***	***12%***	***55%***	***5%***
GFRP_S1	0.1775	95.33	3.70E-04	8.34E-03
GFRP_S2	0.08471	56.25	5.00E-04	5.09E-03
GFRP_S3	0.11988	61.52	6.50E-04	9.71E-03
Mean value	***0.12736***	***71.03***	***5.10E-04***	***7.70E-03***
COV	***37%***	***30%***	***27%***	***31%***

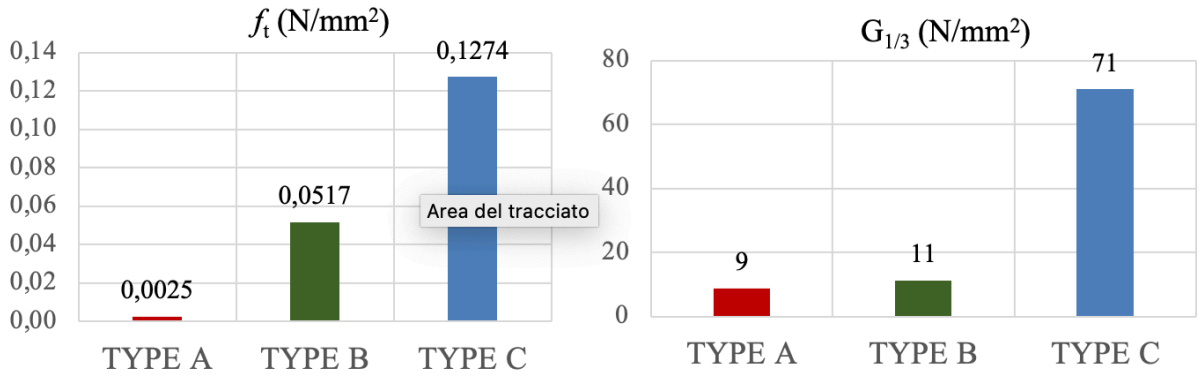

Figure 14. Comparison of (a) the average tensile strengths and (b) secant shear modulus for the three earth masonry specimens under diagonal compression load.

The DIC allowed recovering at each point of the wall the complete displacements and strain fields. For the diagonal compression test the shear strain γ map, evaluated before failure, is presented hereafter since it allows comparing the behavior of the wallettes with and without the reinforcements.

Concerning the bare wallettes, Fig. 15a shows that the maximum values of the shear strain γ occur along the bed joint lines causing a sliding behavior due to the low adhesion at the interface among the earthen blocks. Indeed, in this particular case, the specimens collapse with a total disruption of the masonry structure. Concerning the fir board reinforced specimens (Fig. 15b), the behavior is quite similar to the bare wallettes one with a sliding phenomenon along the bed joints, even though failure has been slowed down by the presence of the reinforcement and of the upper and lower steel plates. Finally, the GFRP reinforced specimens (Fig.15c) showed a better overall monolithic behavior, with the formation of usual vertical cracks along the diagonal strut under compression as in regular masonry wall. This is mostly due to the confinement effect of the GFRP plaster.

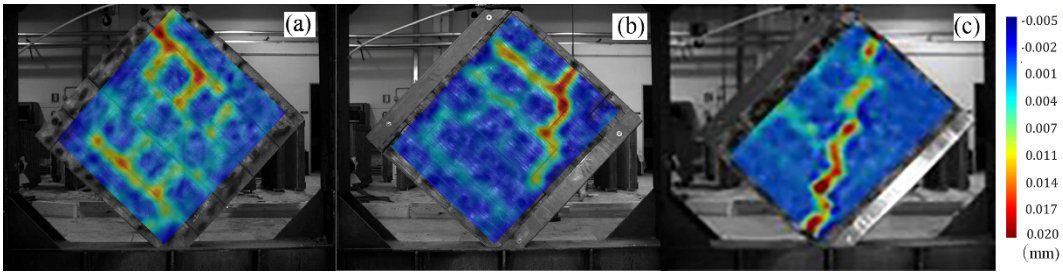

Fig.15 Shear strain γ map under diagonal compression obtained through DIC: (a) bare earth block wallette, (b) fir board reinforced specimen and (c) GFRP reinforced specimen

5. Shear tests with constant compression results on wallettes

The results obtained under s constant compression load of 0.2 N/mm^2 are presented in Fig. 16. In the first part, the curves associated with each type showed a linear trend until the first crack appeared. Then, a plastic region occurred with formation of other diagonal cracks. The trend showed a ductile behavior for the three types of specimen, typical of shear tests with compression. The tensile strength f_t, shear modulus G and shear strain γ of the wallettes (both at 1/3 of maximum shear stress) are reported in Table 5.

The Type C wallettes presented low values of the mean tensile strength (-45%), with respect to the Type B samples (Fig.17a). The latter exhibited a good shear behavior because of the strut mechanism of fir boards opposed to the applied shear force. Instead, the GFRP reinforcement, gave less contribution to the confinement of the wallettes.

The shear modulus of the Type C wallettes notably increased, with respect to the other configurations (Fig.17b). Therefore, for small displacements, this reinforcement has a positive contribution to the stiffness of the system. The increase in stiffness under shear due to the incorporation of wall boards panels was demonstrated by [23]. The authors also clarified that the post elastic deformation capacity of the reinforcement strongly influences the distribution of story forces at increasing seismic actions. Other authors demonstrated that wooden based sheathing panels, such as OSB boards, almost double the final stiffness under shear action [4].

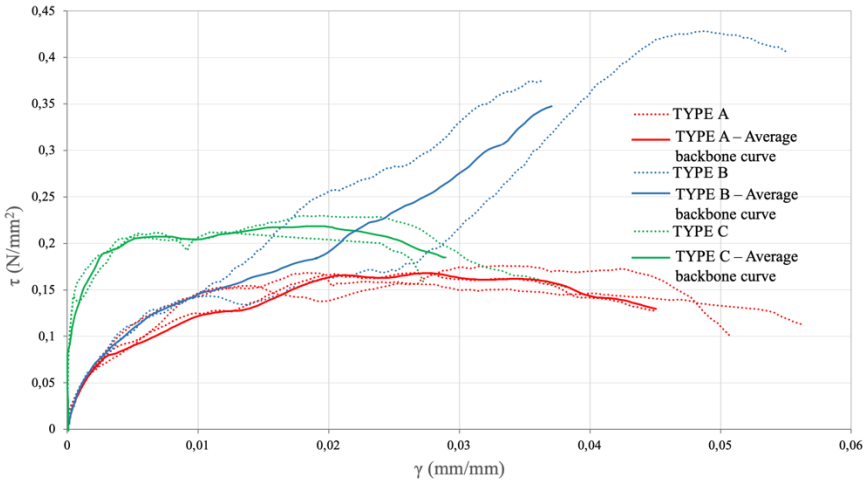

Figure 16. Stress-strain curves of the three types of specimens under shear and compression loads.

Table 5. Tensile strength, shear modulus and ultimate shear strain of the wallettes under a compression load.

Specimen	f_t (N/mm^2)	G (N/mm^2)	γ
SP02_1	0.176	35	0.051
SP02_2	0.168	40	0.045
SP02_3	0.157	39	0.056
Mean value	**0.167**	**38**	**0.051**
COV	**6%**	**7%**	**11%**
SP02_FB1	0.376	43	0.036
SP02_FB2	0.428	40	0.055
Mean value	**0.402**	**41**	**0.046**
COV	**9%**	**5%**	**29%**
SP02_GFRP1	0.212	575	0.027
SP02_GFRP2	0.230	539	0.038
Mean value	**0.22**	**557**	**0.03**
COV	**6%**	**5%**	**24%**

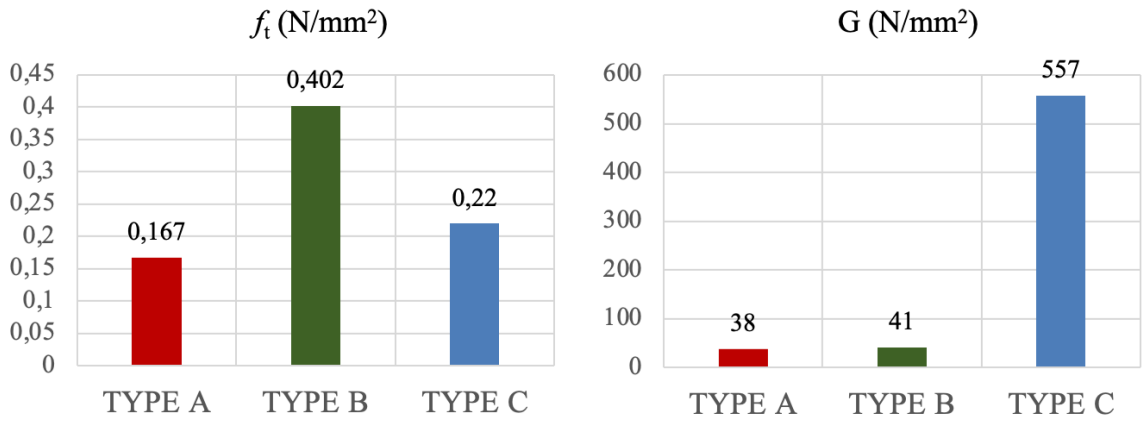

Figure 17. Comparison of (a) the average tensile strengths and (b) shear modulus for the three earth masonry specimens under shear and compression loads.

The DIC allowed recovering at each point of the wall the complete displacements and strain fields. For the shear test with compression the shear strain γ map, just before failure, allows comparing the behavior of the wallettes with and without the reinforcements.

Fig. 18 shows a relevant sliding along the vertical joints for the three cases. This phenomenon has already been pointed out in the vertical displacement maps of the compression test (Fig. 12). The failure mechanism for bare wallettes and GFRP reinforced wallettes (Fig. 18a, c) highlights diagonal staggered fractures following the vertical and horizontal bed joints along the lines of maximum values γ. While, considering the fir board reinforced specimens (Fig. 18b), the rupture has been delayed due to the presence of the boarding, which enters in the strength mechanism of the earthen panel.

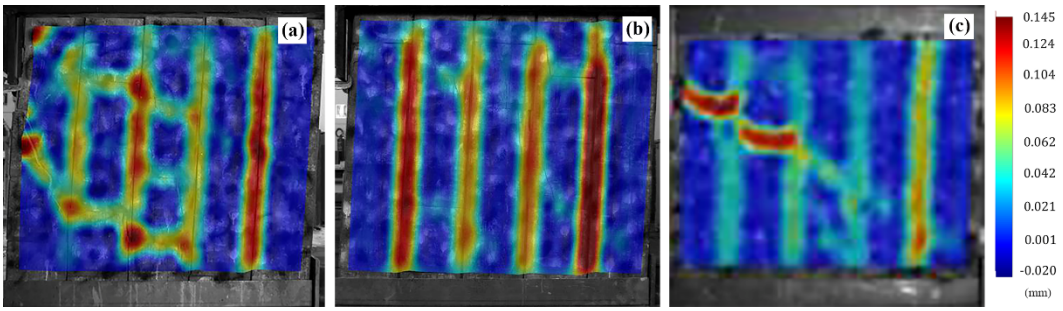

Fig.18 Shear strain γ map in shear tests with constant compression load, obtained through DIC: (a) bare earth block wallette, (b) fir board reinforced specimen and (c) GFRP reinforced specimen

7. Conclusions

An experimental campaign was conducted on 18 wallettes of bare and reinforced earth block masonries, to evaluate the mechanical behavior of these components, generally used as internal/external massive layers in Platform framed structures. The influence on the mechanical behavior of 45-degree angled fir boards sheathing and plaster with a GFRP mesh is investigated through an extensive experimental campaign. Compression tests, diagonal compression tests and shear tests under a constant compression load results were compared with analogous tests results, obtained in [1] for bare walls.

As regards the behavior under axial compression, the results demonstrated that the compressive strength of bare wall specimens is similar to that recorded in reinforced panels since this type of loading does not significantly activate the strength mechanisms of the reinforcements. All the walls behaved as a series of independent slender adjacent columns. The GFRP reinforced specimens had a better overall response, with a more effective collaboration among contiguous members, as commonly occurs in traditional masonries.

As regards the behavior under diagonal compression, as expected the bare wallettes specimens showed the lowest tensile strength, while the GFRP reinforcement had the best outcome. The failure behavior for bare wallettes consisted in a total disruption of the masonry structure, due to the lack of adhesion among the earth blocks. The fir board specimens presented a similar ultimate behavior, even though the collapse is delayed due to presence of the timber boarding. In the case of GFRP plaster strengthening, the overall shear behavior is close to classical masonries with the appearance of a vertical strut under compression.

As regards the behavior under shear with compression load, the data highlighted an increased strength for both the reinforcement types, with the highest value recorded by the fir boards. However, the GFRP mesh showed a significant strength increase also for reduced ultimate strains values and relevant benefices in terms of ductility and lateral load capacity. Moreover, as highlighted by DIC, it conferred to the masonry a more monolithic behavior.

In general, the mechanical performance of the wallettes was improved by the presence of both fir board sheathing and GFRP plaster. The best outcomes were recorded in the GFRP reinforced panels since it determined a relevant increase of strength and stiffness to all the different load configurations. In this case, the mechanical behavior of the earth block wall was close to the one of a classical masonry. The enhancement in

terms of strength, stiffness and lateral load capacity suggests that the configuration involving the GFRP jacketing has the potential to replace the fir board sheathing. Further studies in this direction are, therefore, needed. Future researches will regard the influence of GFRP reinforced massive claddings in the overall response of the timber framed structure.

Aknowledgements

The authors wish to thank TON-GRUPPE® for having provided the material and, particularly, Eng. Marco Tinti for his support on the wallettes manufacturing. The authors wish to thank also Eng. Francesca De Angelis, Eng. Jacopo Costantini and Eng. Marianna Pergolini, who contributed at different levels in the development of the experimental program.

References

[1] F. Stazi, M. Serpilli, G. Chiappini, M. Pergolini, E. Fratalocchi, and S. Lenci, "Experimental study of the mechanical behaviour of a new extruded earth block masonry," *Constr. Build. Mater.*, vol. 244, p. 118368, May 2020.

[2] C. Arya, "Eurocode 5: Design of timber structures," in *Design of Structural Elements*, 2009.

[3] K. Vogrinec and M. Premrov, "Influence of the design approach on the behaviour of timber-frame panel buildings under horizontal forces," *Eng. Struct.*, 2018.

[4] J. M. Branco, F. T. Matos, and P. B. Lourenço, "Experimental in-plane evaluation of light timber walls panels," *Buildings*, 2017.

[5] U. Carusi, F. Riparbelli, and G. Salerno, "Open scientific problems about the Platform Frame constructive system," *Energy Build.*, 2014.

[6] T. Sartori and R. Tomasi, "Experimental investigation on sheathing-to-framing connections in wood shear walls," *Eng. Struct.*, 2013.

[7] F. Stazi, E. Tomassoni, and C. Di Perna, "Super-insulated wooden envelopes in Mediterranean climate: Summer overheating, thermal comfort optimization, environmental impact on an Italian case study," *Energy Build.*, 2017.

[8] L. Miccoli, A. Garofano, P. Fontana, and U. Müller, "Experimental testing and finite element modelling of earth block masonry," *Eng. Struct.*, vol. 104, pp. 80–94, 2015.

[9] A. Dutu, M. Niste, I. Spatarelu, D. I. Dima, and S. Kishiki, "Seismic evaluation of Romanian traditional buildings with timber frame and mud masonry infills by in-plane static cyclic tests," *Eng. Struct.*, 2018.

[10] A. Borri, M. Corradi, R. Sisti, C. Buratti, E. Belloni, and E. Moretti, "Masonry wall panels retrofitted with thermal-insulating GFRP-reinforced jacketing," *Mater. Struct. Constr.*, 2016.

[11] R. Sisti, A. Borri, M. Corradi, and A. Dudine, “Reinforced jacketing of wall panels: A comparative experimental investigation,” in *Key Engineering Materials*, 2019.

[12] N. Torunbalci, E. Onar, and F. Sutcu, “One side strengthening of masonry walls with CFRP,” in *WIT Transactions on the Built Environment*, 2009.

[13] D. Riccadonna, I. Giongo, G. Schiro, E. Rizzi, and M. A. Parisi, “Experimental shear testing of timber-masonry dry connections for the seismic retrofit of unreinforced masonry shear walls,” *Constr. Build. Mater.*, 2019.

[14] A. Borri, R. Sisti, and M. Corradi, “Seismic retrofit of stone walls with timber panels and steel wire ropes,” *Proc. Inst. Civ. Eng. - Struct. Build.*, 2021.

[15] J. Donnini, G. Chiappini, G. Lancioni, and V. Corinaldesi, “Tensile behaviour of glass FRCM systems with fabrics ’ overlap : Experimental results and numerical modeling,” *Compos. Struct.*, vol. 212, no. January, pp. 398–411, 2019.

[16] Q. Piattoni, E. Quagliarini, and S. Lenci, “Experimental analysis and modelling of the mechanical behaviour of earthen bricks,” *Constr. Build. Mater.*, vol. 25, no. 4, pp. 2067–2075, 2011.

[17] M. A. Sutton, F. Matta, D. Rizos, R. Ghorbani, S. Rajan, and D. H. Mollenhauer, “Recent Progress in Digital Image Correlation : Background and Developments since the 2013 W M Murray Lecture,” *Exp. Mech.*, pp. 1–30, 2017.

[18] N. Guerrero *et al.*, “Experimental analysis of masonry infilled frames using digital image correlation,” *Mater. Struct.*, vol. 47, no. 5, pp. 873–884, 2014.

[19] S. H. Tung, M. H. Shih, and W. P. Sung, “Development of digital image correlation method to analyse crack variations of masonry wall,” *Sadhana - Acad. Proc. Eng. Sci.*, 2008.

[20] E. Quagliarini, S. Lenci, and M. Iorio, “Mechanical properties of adobe walls in a Roman Republican domus at Suasa,” *J. Cult. Herit.*, vol. 11, no. 2, pp. 130–137, Apr. 2010.

[21] C. Papanicolaou, T. Triantafillou, and M. Lekka, “Externally bonded grids as strengthening and seismic retrofitting materials of masonry panels,” *Constr. Build. Mater.*, 2011.

[22] C. G. Papanicolaou, T. C. Triantafillou, M. Papathanasiou, and K. Karlos, “Textile reinforced mortar (TRM) versus FRP as strengthening material of URM walls: Out-of-plane cyclic loading,” *Mater. Struct. Constr.*, 2008.

[23] A. Asiz, Y. H. Chui, G. Doudak, C. Ni, and M. Mohammad, “Contribution of plasterboard finishes to structural performance of multi-storey light wood frame buildings,” in *Procedia Engineering*, 2011.